Protein detection on biotin-derivatized polyallylamine by optical microring resonators

Daniela Ullien,[1] Peter J. Harmsma,[2] Shahina M. C. Abdulla,[2] Bart M. de Boer,[2] Duco Bosma,[1] Ernst J. R. Sudhölter,[1] Louis C. P. M. de Smet,[1] and Wolter F. Jager[1,*]

[1]*Department of Chemical Engineering, Delft University of Technology, Julianalaan 136, 2628 BL, Delft, Netherlands*
[2]*TNO, Stieltjesweg 1, 2628CK, Delft, Netherlands*
[*]*w.f.jager@tudelft.nl*

Abstract: Silicon optical microring resonators (MRRs) are sensitive devices that can be used for biosensing. We present a novel biosensing platform based on the application of polyelectrolyte (PE) layers on such MRRs. The top PE layer was covalently labeled with biotin to ensure binding sites for antibodies via a streptavidin-biotin binding scheme. Monitoring the shift in the microring resonance wavelength allows real-time, highly sensitive detection of the biomolecular interaction.

©2014 Optical Society of America

OCIS codes: (130.6010) Sensors; (280.1415) Biological sensing and sensors; (280.4788) Optical sensing and sensors.

References and links

1. W. Bogaerts, P. De Heyn, T. Van Vaerenbergh, K. De Vos, S. K. Selvaraja, T. Claes, P. Dumon, P. Bienstman, D. Van Thourhout, and R. Baets, "Silicon microring resonators," Laser Photon. Rev. **6**(1), 47–73 (2012).
2. A. J. Qavi, A. L. Washburn, J. Y. Byeon, and R. C. Bailey, "Label-free technologies for quantitative multiparameter biological analysis," Anal. Bioanal. Chem. **394**(1), 121–135 (2009).
3. M. S. Luchansky and R. C. Bailey, "High-Q optical sensors for chemical and biological analysis," Anal. Chem. **84**(2), 793–821 (2012).
4. M. J. Bañuls, R. Puchades, and A. Maquieira, "Chemical surface modifications for the development of silicon-based label-free integrated optical (IO) biosensors: a review," Anal. Chim. Acta **777**, 1–16 (2013).
5. F. T. Limpoco and R. C. Bailey, "Real-time monitoring of surface-initiated atom transfer radical polymerization using silicon photonic microring resonators: implications for combinatorial screening of polymer brush growth conditions," J. Am. Chem. Soc. **133**(38), 14864–14867 (2011).
6. M. S. Luchansky, A. L. Washburn, T. A. Martin, M. Iqbal, L. C. Gunn, and R. C. Bailey, "Characterization of the evanescent field profile and bound mass sensitivity of a label-free silicon photonic microring resonator biosensing platform," Biosens. Bioelectron. **26**(4), 1283–1291 (2010).
7. G. Decher, "Fuzzy nanoassemblies: Toward layered polymeric multicomposites," Science **277**(5330), 1232–1237 (1997).
8. R. R. Costa and J. F. Mano, "Polyelectrolyte multilayered assemblies in biomedical technologies," Chem. Soc. Rev. **43**(10), 3453–3479 (2014).
9. http://www.epixfab.eu/
10. D. Taillaert, F. Van Laere, M. Ayre, W. Bogaerts, D. Van Thourhout, P. Bienstman, and R. Baets, "Grating couplers for coupling between optical fibers and nanophotonic waveguides," Jpn. J. Appl. Phys. **45**(8A), 6071–6077 (2006).
11. P. O'Brian, "Silicon PIC packaging," in *ECOC* (Amsterdam, 2013).
12. W. B. Tsai, C. Y. Chien, H. Thissen, and J. Y. Lai, "Dopamine-assisted immobilization of poly(ethylene imine) based polymers for control of cell-surface interactions," Acta Biomater. **7**(6), 2518–2525 (2011).
13. M. Iqbal, M. A. Gleeson, B. Spaugh, F. Tybor, W. G. Gunn, M. Hochberg, T. Baehr-Jones, R. C. Bailey, and L. C. Gunn, "Label-free biosensor arrays based on silicon ring resonators and high-speed optical scanning instrumentation," IEEE J. Sel. Top. Quantum Electron. **16**(3), 654–661 (2010).
14. B. Johnsson, S. Löfås, and G. Lindquist, "Immobilization of proteins to a carboxymethyldextran-modified gold surface for biospecific interaction analysis in surface plasmon resonance sensors," Anal. Biochem. **198**(2), 268–277 (1991).

1. Introduction

Microring resonator (MRR) based sensing [1] is one of the optical label-free technologies available now for highly sensitive detection of biomolecules like proteins or DNA [2, 3]. One

#209835 - $15.00 USD Received 9 Apr 2014; revised 28 May 2014; accepted 31 May 2014; published 27 Jun 2014
(C) 2014 OSA

of the advantages of MRRs is their compatibility with wafer-scale semiconductor fabrication technologies. Essentially, the MRR is a periodic passive wavelength filter, which transmits or absorbs optical signals at specific resonance wavelengths. A fraction of the light in the MRR extends from the MRR surface, decaying exponentially with distance. Changes in the refractive index associated with binding phenomena to the MRR surface cause a shift in the resonance wavelengths, which can be accurately measured. Photons travel multiple roundtrips in the MRR, and consequently have many interactions with the analyte, providing high sensitivity.

This type of devices will reach its full sensing potential for (bio)sensing applications only with highly optimized surface chemistry [3, 4]. For silicon-based optical biosensing, simple physisorption of proteins to the sensor surface has been reported, but for advanced applications surface modification is required. So far, surface modification for biosensing has almost exclusively achieved by covalent functionalization using silane chemistry. Bailey and associates have demonstrated real-time monitoring of several surface modifications on microring resonators, such as polymerization reactions [5] and layer-by-layer (LbL) deposition of polyelectrolytes (PE) [6–8]. The LbL electrostatic polymer deposition was used for evanescent decay profiling, showing a decay length of 63 nm [6].

In this paper, we present a novel method for capturing analyte molecules based on LbL deposition of PEs. This method is based on electrostatic interactions and is very general, as it will work on all charged surfaces. Due to the large decay length of the MRR, around 65 nm, this method allows for the construction of extensive multilayer systems without losing sensitivity. In our approach, the last PE layer is functionalized and this covalent labeling enables the incorporation of a large variety of functional groups at different degrees of functionalization. To the best of our knowledge, surface modification using labeled polyelectrolytes has not been reported for biosensing applications using a MRR or other optical measuring platforms. For the biosensing application demonstrated here, biotinylated polyelectrolyte is used, allowing the subsequent capture of streptavidin as a model protein, see Fig. 1. Figure 1 also gives the structures of polyethyleneimine (PEI), poly(allylamine hydrochloride) (PAH) and poly(sodium styrene sulfonate) (PSS), which were used to prepare the PE stack yielding PEI(PSS/PAH)$_3$.

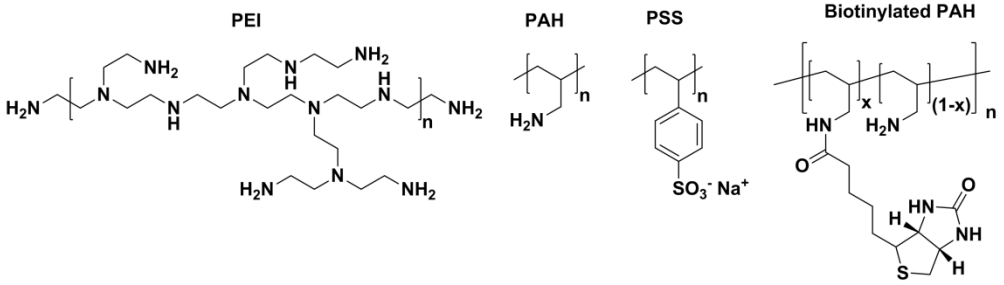

Fig. 1. Polyelectrolytes deposited on MRR device for streptavidin capture.

2. Material and methods

2.1 Materials

Polyethyleneimine (PEI, Mw~25kDa, branched), poly(allylamine hydrochloride) (PAH, Mw~15kDa), poly(sodium styrene sulfonate) (PSS, Mw~70kDa), biotin, N-hydroxysuccinimide (NHS), 1-Ethyl-3-(3-dimethylaminopropyl)carbodiimide (EDC), and streptavidin were obtained from Sigma-Aldrich.

#209835 - $15.00 USD Received 9 Apr 2014; revised 28 May 2014; accepted 31 May 2014; published 27 Jun 2014
(C) 2014 OSA

2.2 Microring resonator

Silicon-On-Insulator (SOI) microring resonators were fabricated in the framework of ePIXfab [9] using a 193 nm deep-UV lithography process. Waveguides are located on a 2.0 µm thick SiO_2 bottom cladding, and have dimensions of 220 nm (height) by 450 nm (width) to support a single transverse electric (TE)-polarized mode at a wavelength of 1550 nm. Optical coupling between access waveguide and ring is provided by Multimode Interference (MMI) couplers having a 50/50 split ratio. The total ring length is 1040 µm, of which 840 µm consists of the waveguide structure described above. The remaining 200 µm is occupied by the MMIs and MMI tapers, and contributes only little to the sensitivity. The ring is folded to a semi-circle, see Fig. 2. To ensure maximum sensitivity, no top layer was applied to the samples, so that only a thin native oxide layer covers the waveguides. Wafers were thinned to 250 µm thickness.

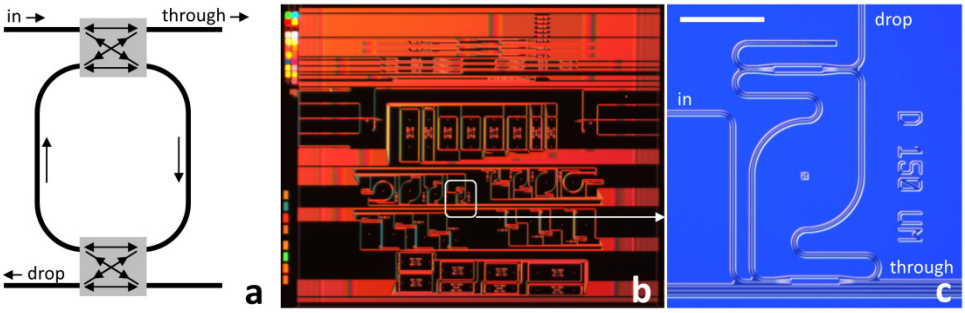

Fig. 2. (a) Schematic representation of MRRs, showing a ring-shaped waveguide, with optical couplers to input, 'through' output and 'drop' output. (b) Microscopic photograph of generic MRR test chip (6x6 mm). (c) Microscope photograph of the device selected for these tests. The scale bar indicates 100 microns.

We use out-of-plane grating couplers [10] to couple light in and out of the MRR. These grating couplers, designed to couple TE polarized light into the chip, are mature and standardized building blocks in the ePIXfab platform. At the time of design, TM couplers were not yet validated, which was the main reason to design our system for TE polarization only. To permanently mount fibers to the chip, we use fibers having 40° angled facets mounted in-plane with the chip [11], see Fig. 3(a). A thermal conductive glue is used for bonding the chip to an aluminum plate for temperature stabilization and assembly robustness. A home-built flow cell made from PMMA, see Fig. 3(b) is glued on top of the chip using a UV curable glue (NOA61, Norland Products). With a pumping rate of 90 µl / minute, the flow rate of the liquid at the resonator sensing area is 1 mm/sec, which is in the laminar flow regime for water.

#209835 - $15.00 USD Received 9 Apr 2014; revised 28 May 2014; accepted 31 May 2014; published 27 Jun 2014
(C) 2014 OSA

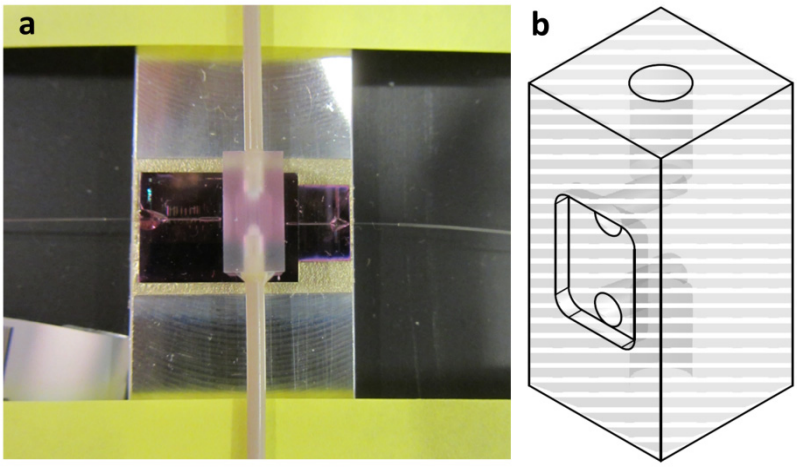

Fig. 3. Top view of assembled MRR sensor (a), showing the flow cell glued on the chip, with tubing extending upwards and downwards, and in-plane mounted fibers extending to the left and right, and (b) schematic of the flow cell.

Figure 4 shows typical MRR transmission spectra before and after fiber mounting. Fiber mounting introduces about 3 dB extra loss of optical power per fiber connection due to non-optimal alignment. Upon mounting the spectra become cleaner because the transparent UV epoxy between fiber and grating coupler suppresses residual reflections. Ring performance parameters such as Free Spectral Range (FSR, 500 pm) and the on-off ratio (14 dB) remain the same. The FSR agrees well with the estimated 520 nm as follows from $FSR = \lambda^2/n_g L$, with λ the wavelength (1531 nm), n_g the waveguide group index (4.337), and L the ring length (1040 μm). The small deviation can be explained by small waveguide width deviations, and by the different effective group index of the MMI couplers.

The overall loss is in the order of 21 dB. Each grating coupler causes 5 dB loss, and the 7 mm of access waveguides another 2 dB loss in air. The MRR insertion loss is 1 dB, a 3-dB fiber-optic splitter, see Fig. 5, adds up to an expected loss of 16 dB. The remaining 5 dB is caused by extra waveguide loss due to absorption by the water, and by non-optimal alignment even prior to gluing.

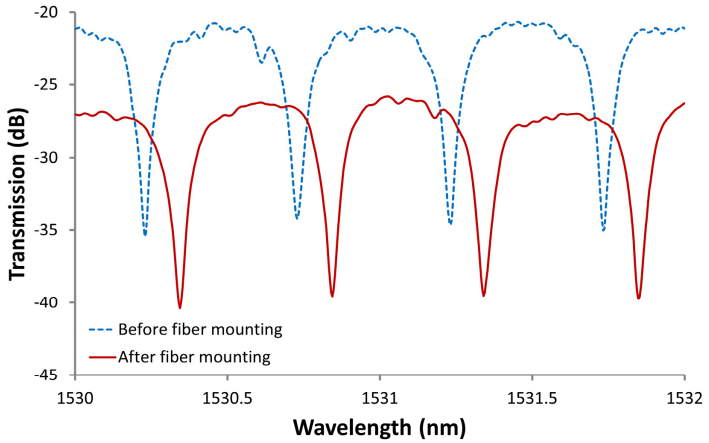

Fig. 4. Transmission spectra of the MRR.

#209835 - $15.00 USD Received 9 Apr 2014; revised 28 May 2014; accepted 31 May 2014; published 27 Jun 2014
(C) 2014 OSA

2.3 Optical setup

During the binding experiments, we continuously measure the MRR spectra, and post-process the data to obtain the resonance wavelengths as a function of time. The spectra are measured by scanning the wavelength of a tunable laser (Agilent 81960A), and measuring the power transmitted by the MRR using a detector (Agilent N7744), see Fig. 5(a). A polarization controller (HP 11896A) sets the polarization to TE at the chip, thereby maximizing the transmission. A typical measurement over 2 nm takes 0.7 seconds.

In order to verify that the MRR response did not shift rapidly by more than the Free Spectral Range within a measurement interval, we optionally include a second laser (New Focus 6262), see Fig. 5(b) and fix its wavelength to match the reflection wavelength (1529.8 nm) of a temperature insensitive Fiber Bragg Grating (FBG). The signal from this second laser 2 is reflected by the FBG, and routed to detector 2 by the optical circulator. The scanning range of tunable laser 1 is chosen not to include the FBG reflection wavelength, and this signal is transmitted by the FBG to detector 1. This system provides two independent simultaneous measurements:

1) A wavelength scan (laser 1, detector 1), providing accurate MRR wavelength shifts. Data acquisition rate is in the order of 1 Hz.

2) A transmission measurement at fixed wavelength (laser 2, detector 2). Each MRR wavelength shift by one FSR causes a minimum and maximum of the detector signal. Data acquisition rate is in the order of 50 kHz, so that high-speed large shifts can be monitored by counting the detector signal minima and maxima.

Combining the result of these two data sets, accurate wavelength shifts are obtained in which a full FSR shift will be spotted accurately.

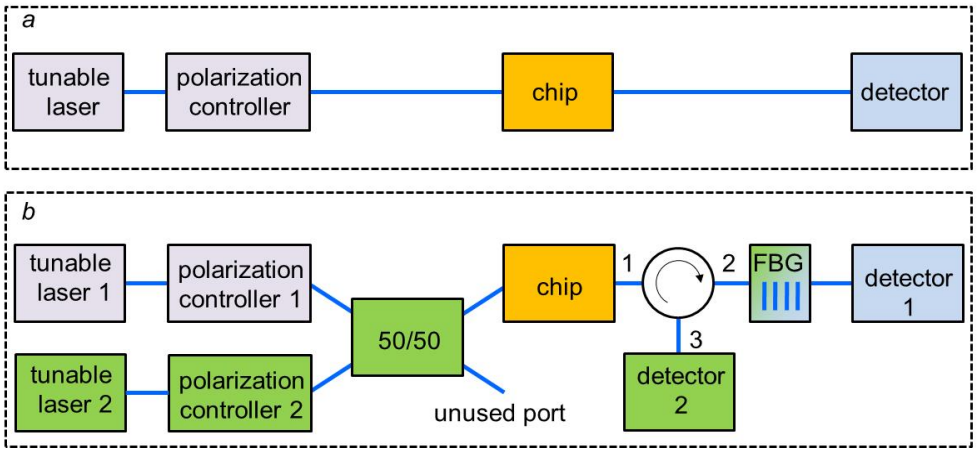

Fig. 5. Optical setup: using a single scanning laser source (a) and using an additional fixed laser source, with the optical path indicated in green (b). FBG stands for Fiber Bragg Grating.

2.4 Synthesis of biotinylated PAH

Biotinylated PAH was synthesized by covalent attachment of biotin to PAH via a carbodiimide-activated coupling reaction. The synthesis was adapted from Tsai et al. [12]. 6% biotinylated PAH was synthesized by adding 500 mg PAH, 130 mg biotin, 166 mg EDC, and 61.5 mg NHS in 70 ml deionized water (DI) and reacting at room temperature for 3 days while stirring. The unreacted biotin was removed by dialysis (Mw cut off ~7 kDa) against DI water for 2 days with refreshing every 12 h. To evaluate the biotin grafting density, biotinylated PAH was freeze dried and analyzed by proton nuclear magnetic resonance (^{1}H-

#209835 - $15.00 USD Received 9 Apr 2014; revised 28 May 2014; accepted 31 May 2014; published 27 Jun 2014
(C) 2014 OSA

NMR). Using the integrated values of the two peaks at 4.4 and 4.6 ppm in the proton NMR spectrum, which originate from the two bridgehead protons of biotin, the labeling was calculated to be 2.5%, 6% and 9% biotin load of the PAH polymer.

2.5 Polyelectrolyte deposition and streptavidin immobilization

PE layers were formed by subsequently flushing the flow-cell with 1 mg/ ml PEI, PSS and PAH in 150 mM NaCl pH = 5.5 solution for 4 min at a pumping rate of 90 µl/min. The last bound PE layer was a biotinylated PAH added using a concentration of 1 mg/ ml in 150 mM NaCl pH = 5.5. After each polymer deposition, the chip was flushed with 150 mM NaCl for 4 min. The constant flow conditions were maintained with a syringe pump model 33 from Harvard apparatus.

If the flow for the first PSS layer deposition is continued for 15 min., then the following layers exhibit a very unstable behavior. The optimum deposition time was found to be 4 min.

After PE deposition, 1 or 10 µg/ ml of streptavidin in NaCl pH = 5.5 was flushed through the flow-cell for 1 h. NaCl solutions were adjusted to the required pH by adding small amounts of concentrated NaOH (aq.) or HCl (aq.). The solution pH was monitored (and re-adjusted when required) with a Metrohm 827 pH Lab meter (Metrohm Applikon, The Netherlands).

3. Results

3.1 MRR sensitivity

Using the setup shown in Fig. 5(b) we counted the transmission minima and maxima while the ring resonator becomes wet. When aqueous NaCl reaches the MRR device, first the optical power drops a bit due to losses of the wetted input waveguide. The solution reaches the ring at 11.3 sec, shifting the resonances, see Fig. 6. The wetting of the ring resonator takes about 0.3 sec. The fringes are generated at a rate of up to 2 fringes per ms, the typical total number of fringes is 50, see Fig. 6. This corresponds to a wavelength shift of 25 nm for an ambient refractive index change of 0.33, or a sensitivity of 75 nm/RIU. A commercial waveguide simulation tool (Photon Design Fimmwave) predicts a sensitivity of dn_{eff}/dn_{amb} = 0.197, with n_{eff} the effective index of the waveguide, and n_{amb} the ambient refractive index. Using $d\lambda/d_{namb} = (\lambda/n_g)\cdot dn_{eff}/dn_{amb}$ with λ the wavelength and n_g the group index, we expect a sensitivity of 70 nm/RIU. The observed value is slightly higher, in spite of the fact that the MMI couplers do not contribute significantly to the sensitivity. Higher sensitivity values reported in literature (for example 163 nm/RIU [13]) can only be achieved using TM polarization. We calculate a TM sensitivity in the order of 220 nm/RIU for our waveguide structure.

#209835 - $15.00 USD Received 9 Apr 2014; revised 28 May 2014; accepted 31 May 2014; published 27 Jun 2014
(C) 2014 OSA

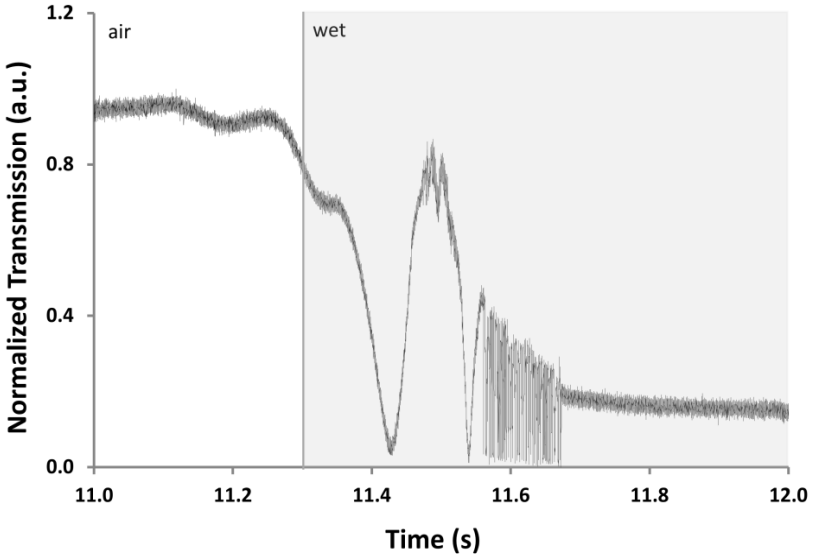

Fig. 6. Fringe counting during the transition of MRR from air to NaCl solution.

3.2 MRR response to PEs deposition

The wavelength shift of the MRR upon the addition of PE layers is shown in Fig. 7. In Fig. 7(a) the sequential addition of the different polyelectrolytes, being PEI, PSS, PAH, PSS, PAH, PSS and biotinylated PAH is shown. On the horizontal-axis we plot the time when the PEs or 0.15 M NaCl aqueous solution were added to the flow-cell as indicated by the vertical lines in the Fig. 7(a). It takes 1.5 min. to observe the shift in the case of PEs, due to the time for the solution to pass through the tubing to reach the flow-cell (dead volume ≈135 µl). Wavelength shifts observed upon polyelectrolyte addition are typically in the order of 0.3 to 0.6 nm, which is significantly larger than values reported earlier with the same polymers [6]. Measurements of the thickness of dry PAH/PSS bilayers by elipsometry, also indicate a significantly larger layer thickness of 5.4 nm.

Also noteworthy, and different from previously reported cases, is the very small 0.02 nm shift that is observed upon rinsing with aqueous NaCl solution. This indicates that the polyelectrolyte layers are firmly attached and are not easily washed away.

The wavelength shifts inflicted by each PE attachment from 6 different experiments are represented in Fig. 7(b). Figure 7(b) clearly shows that wavelength shifts induced by the first two PE attachments, from the first PEI layer and the first PSS layer, exhibit large variations. These variations exceed the variation in sensitivity between individual MRRs, which is in the order of 10% (measured with NaCl solution), and may be due to the initial cleanliness of the oxide surface. The variations in wavelength shifts decrease with the attachment of the following layers, with a notable exception for the last PAHb layer, *vide infra*. It is clearly visible that the wavelength shifts upon attachment of PSS layers (0.50 ± 0.05 nm) are substantially larger than those observed for PAH layers (0.29 ± 0.04 nm). The wavelength shift induced by the addition of biotinylated PAH (0.44 ± 0.08 nm) is significantly larger than the typical PAH shift. There is a clear difference between the 2.5% biotinylated PAH (the two lower points) which have an average response of 0.34 nm and the rest of the biotinylated series with an average of 0.49 nm. This implies that the covalent attachment of biotin to the PAH has a positive effect on the binding of this polyelectrolyte, despite the decreased charge density of this polymer.

#209835 - $15.00 USD Received 9 Apr 2014; revised 28 May 2014; accepted 31 May 2014; published 27 Jun 2014
(C) 2014 OSA

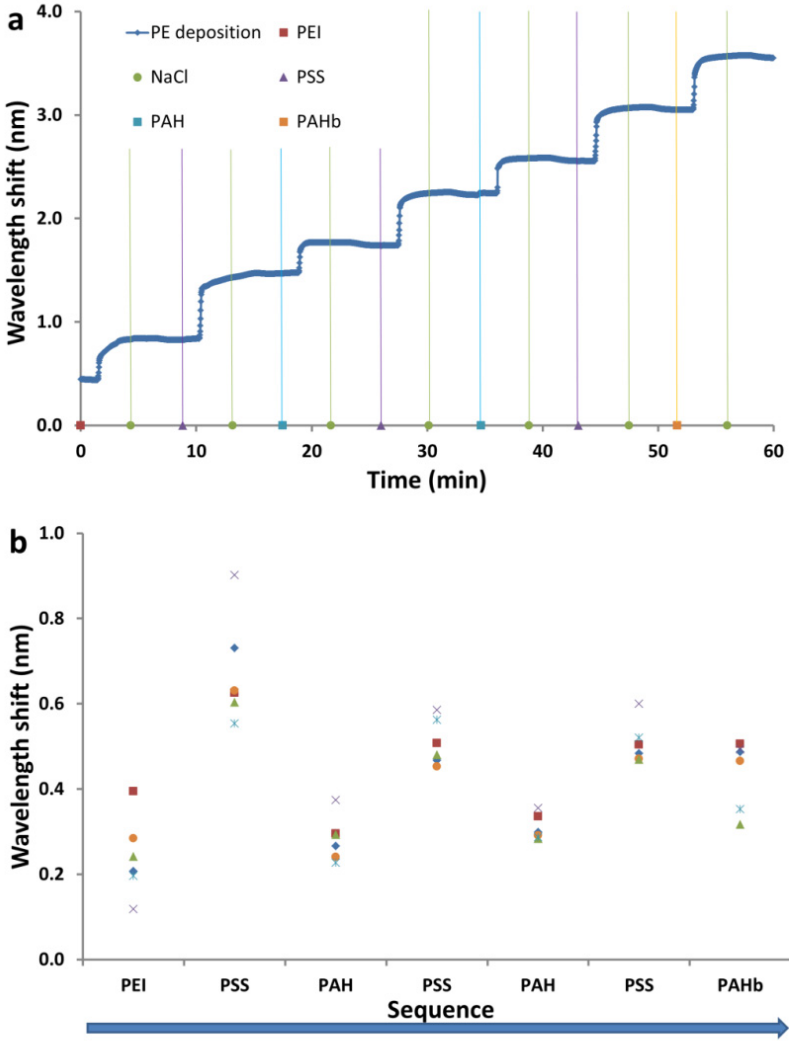

Fig. 7. (a) Optical response of the MRR to the addition of PE layers. (b) Wavelength shifts of MRRs upon PEs addition for 6 individual devices.

3.3 Biotinylated PAH/ streptavidin

The last layer of PE on the MRR was biotinylated PAH, which can bind streptavidin. We used streptavidin as a model protein for measuring the binding event between the analyte and the underlying surface. The response of the ring resonator upon injection of streptavidin solutions shows that the time at which the streptavidin starts to attach, does not correlate with the injection time. While the polyelectrolytes all started to grow at exactly 1.5 minutes after injection, streptavidin growth starts much later, at 7 to 15 minutes after injection. This phenomenon is attributed to non-specific binding of the protein to the tubing and the interior of the flow cell, which consumes the protein before it reaches the active surface of the ring resonator.

In Fig. 8 we have normalized the raw data by starting all traces at the origin at the moment the streptavidin attachment begins. Figure 8 clearly demonstrates that the magnitude of the

#209835 - $15.00 USD Received 9 Apr 2014; revised 28 May 2014; accepted 31 May 2014; published 27 Jun 2014
(C) 2014 OSA

wavelength shift, ranging from 0.45 to 0.9 nm is comparatively large. This wavelength shift, which is proportional to the amount of streptavidin attached, is a function of the degree of biotinylation of the underlying PAH layer and, to a lesser extent, to the streptavidin concentration.

The best results, implying faster growth, and the formation of a denser streptavidin layer, are obtained by using PAH with 6% biotin attached. When 10 µg /ml streptavidin is injected the layer growth is fast and 80% is finished within 5 minutes. Using a 1 µg /ml streptavidin solution the growth is much slower, and clearly divided in two regimes; fast growth during the first 15 minutes, and a much slower growth afterwards. Nevertheless, the total wavelength shift approaches the same value after 1 hour, indicating that the amount of streptavidin attached is independent of the streptavidin concentration. It was also demonstrated that rinsing with aqueous NaCl solution did not remove the bound streptavidin (not shown).

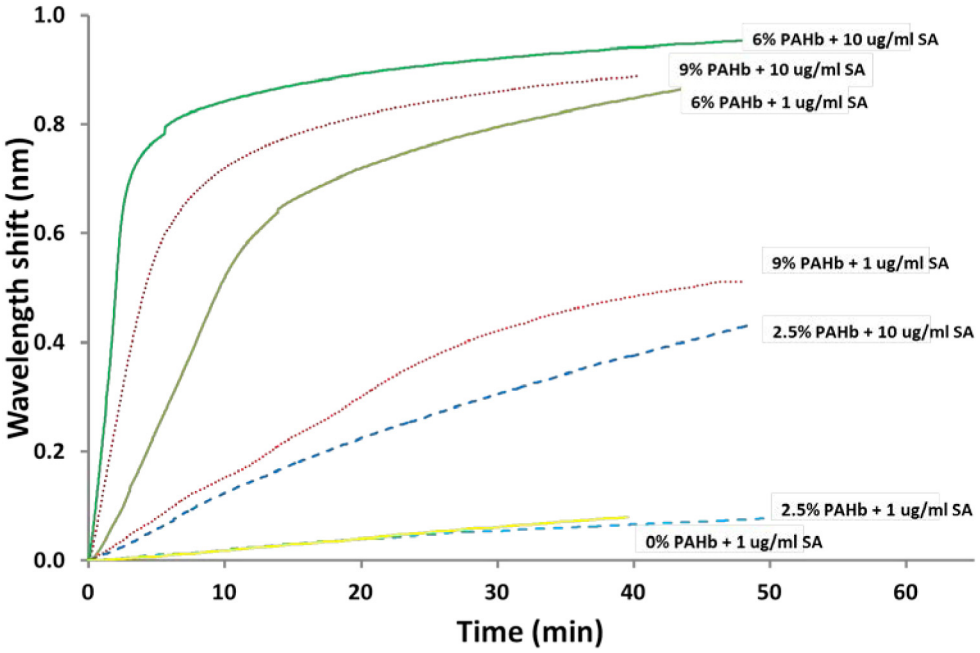

Fig. 8. Normalized MRR shifts as a response to the addition of 1 and 10 µg/ ml streptavidin. Data was taken at a sampling rates between 0.8 and 1.4 Hz, clearly faster than the timescale of the binding process.

For the 9% biotinylated PAH layer, the amount of streptavidin attached, and the rate of streptavidin attachment are lower. Using 10 µg /ml streptavidin solutions a fast growth was observed during the first 5 minutes, followed by a much slower growth afterwards like in the case with 6% biotinylated PAH. Using 1 µg /ml streptavidin solutions, the growth is slower and the amount of streptavidin attached after one hour is much lower when lower concentrations of streptavidin are used. Whether the final degree of loading depends on the streptavidin concentration cannot be concluded from our data.

For the 2.5% biotinylated PAH layers the slowest streptavidin attachment was observed. Using the 10 µg /ml streptavidin solution, the slowest growth was observed among different percentages of biotinylation. For the 1 µg /ml streptavidin solution the rate and the extend of streptavidin attachment were very low, and similar to those of non-specific binding to a blank, non-biotinylated, PAH sample.

These results clearly indicate that efficient and strong streptavidin binding to the biotinylated PAH can be achieved, but that streptavidin also binds non-specifically to other surfaces. This non-specific binding may also explain why the initial slope during the

#209835 - $15.00 USD Received 9 Apr 2014; revised 28 May 2014; accepted 31 May 2014; published 27 Jun 2014
(C) 2014 OSA

streptavidin binding does not scale with the streptavidin concentration, as expected [14]. In order to make devices that do not waste precious proteins by non-specific binding, it is necessary to prevent this binding of streptavidin by blocking the non-specific binding sites by an inactive protein, e.g. bovine serum albumin or other bio-repellent species.

4. Discussion

We have shown that a 7-layer polyelectrolyte film, composed of PEI, PSS, PAH, PSS, PAH, PSS and biotinylated PAH can be produced in a reproducible fashion. The observed wavelength shifts upon PE deposition are large and the deposited layers are very stable. Layer detachment by rinsing with aqueous NaCl is hardly observed. This is in contrast to the case of Luchansky et al. [6], where rinsing with Tris buffer causes substantial detachment of PE layers, in particular the PAH layer. This is most likely due to competition of the ammonium ions of the Tris buffer and those of the attached PAH molecules.

The covalent attachment of biotin to the upper PAH layer, turns out to be a versatile and efficient method for producing a biotin-functionalized surface. Streptavidin attachment was observed for PAH with a 2.5, 6 and 9% degree of functionalization. However, kinetics of streptavidin binding and final layer density were not proportional to the degree of PAH biotinylation. Remarkably, the best results, in terms of rate and extent of streptavidin attachment, were obtained with the intermediate degree of biotin functionalization, i.e. 6%.

Non-specific binding of streptavidin to exposed surfaces is significant and has a pronounced effects on our experiments. Due to non-specific streptavidin binding, the streptavidin concentration profile in the solution above the ring resonator is not known. Therefore the initial slope during the streptavidin binding does not scale with the administered streptavidin concentration. Also, subsequent binding events to obtain a useful biosensor by immobilization of antibodies against a clinically-relevant analyte will take place on the non-specifically bound streptavidin and lead to waste of precious materials and loss of sensitivity.

5. Conclusion

We have demonstrated that the silicon optical microring resonator (MRR) is a highly sensitive, reliable and user friendly device for investigating surface modification and the subsequent construction of biosensors. Using this device we demonstrated that PEs deposition from aqueous NaCl solution results in stable PE layers, which exhibit negligible PE detachment during the rinsing step. We have shown that a stable 7-layer polyelectrolyte film, composed of PEI and alternated layers of PSS and PAH can be produced in a reproducible fashion. Employing biotinylated PAH as the last PE layer in this architecture, has been demonstrated as a suitable technique for protein deposition on MRRs.

Deposition of streptavidin on these biotinylated surfaces, based on kinetics and final layer density, worked best for PAH layers with an intermediate, 6%, degree of biotinylation. For follow-up experiment we intend to use the streptavidin functionalized PE architecture as a universal platform for the development of biosensors.

Acknowledgments

The Dutch Technology Foundation STW is acknowledged for financial support (project number: 10255).

#209835 - $15.00 USD Received 9 Apr 2014; revised 28 May 2014; accepted 31 May 2014; published 27 Jun 2014
(C) 2014 OSA